Food Hydrocolloids 154 (2024) 110130

Contents lists available at ScienceDirect

Food Hydrocolloids

journal homepage: www.elsevier.com/locate/foodhyd

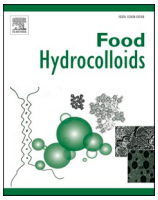

Dysphagia food: Impact of soy protein isolate (SPI) addition on textural, physicochemical and microstructural properties of peach complex gels

Jin Xie [a,b], Jinfeng Bi [a,*], Jacquet Nicolas [b], Blecker Christophe [b], Fengzhao Wang [a], Jian Lyu [a,**]

[a] Institute of Food Science and Technology, Chinese Academy of Agricultural Sciences, Key Laboratory of Agro-products Processing, Ministry of Agriculture and Rural Affairs, Beijing, 100193, China
[b] University of Liège, Gembloux Agro-Bio Tech, Unit of Food Science and Formulation, Avenue de la Faculté d'Agronomie 2B, Gembloux, B-5030, Belgium

ARTICLE INFO

Keywords:
Peach pulp
Soy protein isolate
Dysphagia
Rheology
Texture

ABSTRACT

In this study, dysphagia-friendly diets were prepared based on the interaction between polysaccharides from peach, namely Meirui (MR), Yangshan (YS) and Cons758 (Cons), and soy protein isolate (SPI). MR-alcohol insoluble residues (AIR) and YS-AIR were low methoxylated polymers, while Cons-AIR was high methoxylated polymer. According to the international dysphagia diet standardization initiative, YS-SPI and MR-SPI could be qualified as level 5-minced/moist dysphagia diets. Following SPI addition, the apparent viscosity, G′ and G″ of peach pulp-SPI complexes were significantly increased. At the shear rate of 10 s^{-1}, corresponding to oral processing, MR-SPI performed the highest apparent viscosity (35.2 Pa s), followed by YS-SPI (33.5 Pa s). Additionally, the SPI-treated strategy pronounced improved the hardness, springiness, adhesiveness and chewiness of complexes. Both YS-SPI and Cons-SPI showed the reduced particle size, alongside the uniform distribution, owing to the strong hydrogen bonding and electrostatic interaction between peach pulp substances and SPI, which was confirmed by FT-IR result. The biggest ζ-potential value (−23.55 mV) was found in YS-SPI. Meanwhile, compared with peach pulps, the highest increase ratio (87.94%) of water holding capacity was depicted in MR-SPI. LF-NMR analysis revealed immobilized water was dominant in peach pulp-SPI. The results suggested that MR was promising for the optimal choice to form gel food for people with swallowing problems.

1. Introduction

Over 590 million people worldwide are living with dysphagia. Currently, the dysphagia diet consists of mashed or thick liquids (IDDSI, 2019), which are poorly attractive and unappetizing. To improve individual lives, dysphagia foods with various textures and shapes have garnered wide concern and require further research and development. Additionally, the standardized method to define and describe texture-modified foods and thickened liquids for individuals with swallowing difficulty has been established by the international dysphagia diet standardization initiative (IDDSI), which clearly promoted the development of sustainable dysphagia food (Ekonomou et al., 2024).

Based on the gelling properties, polysaccharides, protein and sodium alginate have been widely applied in semi-solid food. Especially, the interaction between polysaccharides and protein that contributed to food's structure, stability, texture, and mouthfeel has attracted considerable attention. Plant proteins, as a sustainable functional food ingredient, are increasingly being valued, owing to consumers' preferences for healthy and environmentally sustainable diets. Soy protein isolate (SPI), with excellent emulsifying, foaming, gelling and film-forming properties, has been widely used as an ingredient in compound food systems (Ma et al., 2019). Recently, numerous researches focused on the formation of gel systems consisted of protein and polysaccharides (He, Liu, Zhao, Li, & Wang, 2021; Liu et al., 2023). However, few studies have been conducted on fruit pulp and plant protein, which could provide a new strategy for comprehensive utilization of the nutritional components of fruit pulp. Fruit pulp, as a good resource of polysaccharides, could form gels with proteins based on its colloidal property (Ma et al., 2019). Therefore, the gel-like substance formed by

Abbreviations: SPI, Soy protein isolate; LMP, Low methoxylated polymers; AIR, Alcohol insoluble residues; LF-NMR, Low field nuclear magnetic resonance; FT-IR, Fourier transform infrared spectroscopy.

* Corresponding author.
** Corresponding author.
E-mail address: bjfcaas@126.com (J. Bi).

https://doi.org/10.1016/j.foodhyd.2024.110130
Received 30 November 2023; Received in revised form 21 April 2024; Accepted 22 April 2024
Available online 23 April 2024

polysaccharides and proteins with good flowability, viscosity and elasticity are suggested to efficiently decrease the risk of dysphagia (Mao et al., 2023). Additionally, the complexation process and texture properties of fruit pulp-protein gels are varied from the differences in physicochemical properties of fruit pulp substances. The structure features of polysaccharides, such as degree of esterification (DE) and extent of branching of pectin, significantly affected the texture quality of yellow peaches (Wang, Lyu, Xie, & Bi, 2023). Furthermore, pectin, as a negative charge polysaccharide can bind with positive charge proteins through strong electrostatic attraction or non-covalent bond, which is supported to format protein-polysaccharide complexes (Ma et al., 2020; Souza & Garcia-Rojas, 2015). However, with both carrying net charges (polysaccharides and protein), insufficient electrostatic interaction can limit complex coacervation, while excessive charges may result in precipitation or repulsion. Generally, compared with high methoxylated polymers (HMP), low methoxylated polymers (LMP) with more negative charges and more free carboxyl groups exhibit higher charge density, which significantly promoted the formation of protein-pectin complex (Jones, Lesmes, Dubin, & McClements, 2010). However, LMP with high amounts of galacturonic acid (GalA) could promote the repulsion among carboxylate anions, which might have an antagonist effect on the formation of polysaccharides-protein gels (Warnakulasuriya, Pillai, Stone, & Nickerson, 2018).

In this study, SPI selected as food matrices was added in peach pulps to produce gel complex for people with swallowing disorders. IDDSI tests were applied to evaluate the texture properties and define the level of the texture-modified gel complex. Furthermore, texture, rheology, particle size, water holding capacity (WHC) and microstructure were studied to provide a more complete characterization of the compound gels. ζ-Potential, LF-NMR and FTIR were measured to better understand the formation mechanism of gels. Additionally, interactions among biopolymers in the compound gel systems were also discussed, which would be helpful for facilitating the development of dysphagia food.

2. Materials and methods

2.1. Materials

Soy protein isolate (SPI, content ≥90%, analytical grad) was purchased from Shanghai Yuanye Bio-Technology Co. Ltd. Non-melting peach (*Cons758*), melting peach (*Yangshan*), and crisp peach (*Meirui*) purchased from the local Hualian supermarket (Beijing, China) were selected as the test material.

2.2. Preparation of peach pulps

Cons758, *Yangshan,* and *Meirui* were washed and sliced after removing the kernels and ground for 2 min by a blender (Supor, Co. Ltd, Zhejiang, China), respectively. The obtained peach pulps were stored at 4 °C until use (less than 48 h).

2.3. Preparation of peach pulp gels and peach pulp-SPI gels

Peach pulp gels were prepared as the following procedure: *Cons758*, *Yangshan,* and *Meirui* pulps were respectively stirred using a homogenizer (RW 20 digital, IKA, German) with 300 rpm/min for 1 min and then heated to 95 °C in a water bath (HH–4B, Changzhou Ronghua Instrument Co., Ltd, Changzhou, China) for 30 min. Peach pulp gels prepared by *Cons758*, *Yangshan,* and *Meirui* pulp were marked as Cons, YS, and MR, respectively.

For peach pulp-SPI gels: SPI was first mixed with three peach pulps at a weight ratio of 9: 1, respectively. The peach pulp-SPI complexes were homogenized for 1 min with 300 rpm/min to avoid the possible accumulation of SPI particles during the preparation. After, the complexes were treated at 95 °C in a water bath for 30 min to get the peach pulp-SPI gels, which were labeled as Cons-SPI, YS-SPI and MR-SPI, respectively. Further, samples were cooled down at room temperature and then refrigerated at 4 °C overnight for the following analyses.

2.4. IDDSI

The IDDSI framework consisted of 8 levels (0–7). Level 0–2 was referred to drink, level 3–4 was between drink and food, and level 5–7 was labeled as transitional foods (Fig. 1). Thick drinks and fluid foods (Levels 3 and 4) were tested by checking if they pass through the tines/prongs of a fork. In this study, all samples could not go through the 10 mL slip tip syringe while could pass the fork drip test were identified as higher than level 3 (Fig. S1). The spoon tilt and fork pressure test are used to determine samples in levels 4 and 5 (IDDSI, 2019). According to the IDDSI framework and the properties of samples, the spoon tilt test and the fork pressure test were performed to evaluate the stickiness (adhesiveness) and the ability of the sample to hold together (cohesiveness). The spoon tilt test was tested as follows: firstly, scoop a teaspoon of the sample and hold the spoon steady above a plate, after that tilt the spoon sideways gradually. The fork pressure test was tested as follows: a fork with a 4 mm gap was pressed down the samples by using a consistent force. The front-end of fork handle was pressed with the thumb until nail turned white, and then observed the samples on the surface of the fork and evaluate whether they could pass through the fork gap. The particle size with 2–4 mm of food was safe for patients with dysphagia. Therefore, the standard gap with 4 mm between the forks' teeth was an effective tool for measuring the particle size of food (Xing et al., 2022).

2.5. AIR (alcohol insoluble residues) isolation

AIR was isolated from peach pulps according to Wang et al. (2023) with some modifications. Peach pulp (100 ± 0.2 g) was mixed with 500 mL of 70% (v/v) ethanol for 2 h by a disperser (T25 digital ultra turrax, IKA, German), which was repeated for three times until the ethanol filtrate was colorless. Afterward, residue was mixed with 300 mL of acetone for 5 min. At last, resulting residue, labeled as AIR, was dried overnight at 40 °C and then stored in a desiccator for future use.

2.6. Preparation of pectin fractions

Pectin fractions, namely water-soluble pectin (WSP), chelator

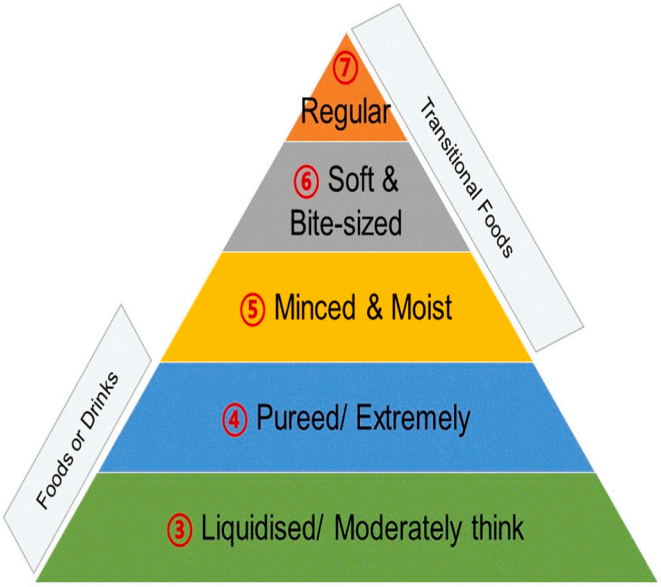

Fig. 1. The international dysphagia diet standardization initiative (IDDSI) framework.

soluble pectin (CSP), and sodium carbonate soluble pectin (NSP) isolated from AIR were prepared based on our previous study (Wang et al., 2023). AIR (1.00 ± 0.02 g) was mixed with 180 mL Milli-Q water and kept at 100 °C for 10 min with constant stirring. The filtrate was dialyzed using Milli-Q water for 72 h and marked as WSP fraction. The residue was mixed with 180 mL 0.05 mol/L cyclohexane-trans-1, 2-diamine tetra-acetic (CDTA) in 0.1 mol/L potassium acetate for 6 h with constant stirring, pH was adjusted at 6.5 by adding 0.1 mol/L HCl at room temperature. The filtrate was dialyzed with 0.1 mol/L NaCl for 36 h, then with Milli-Q water for another 36 h, which was named CSP fraction. The above residue was extracted with 180 mL 0.05 mol/L Na_2CO_3 containing 0.2 mol/L $NaBH_4$ at 4 °C for 16 h under constant stirring, followed by re-incubation at room temperature for another 6 h. The filtrate was dialyzed with Milli-Q water for 72 h and marked as NSP fraction. A freeze dryer (BLK-0.5, Jiangsu BoLaiKe Refrigeration Science and Technology Development Co., Ltd., Jiangsu, China) was used to obtain the WSP, CSP, and NSP fractions.

2.7. Degree of esterification (DE)

DE was usually reported as methoxyl content of total pectin, namely, the extent to which carboxyl groups in the galacturonan chain exit as the methyl ester. The amount of methanol and Galacturonic acid (GalA) were conducted on a UV detector (UV-2550, Shimadzu, Japan) at 412 nm and 520 nm, respectively, according to the method described by Milošević and Antov (2022). AIR (20.0 ± 0.2 mg) was dissolved in Milli-Q water (8 mL) and sonicated for 10 min, which was then mixed with aryl-alcohol oxidase (1 U/mL) and kept at 25 °C for 15 min with the occasional shaking. Subsequently, the sample was mixed with the pentanedione (2 mL) and kept at 58 °C in a water bath for 15 min with occasional shaking. Additionally, methanol (0–24 μg/mL) was used as an internal standard.

$$DE\% = \frac{N_{MeOH}}{N_{GaLA}} \times 100\% \quad (1)$$

where, N_{MeOH} was the moles of methanol, mol; N_{GaLA} was the moles of galacturonic acid, mol.

2.8. Monosaccharides

An ICS-3000 Ion Exchange Chromatography system (Dionex, USA), equipped with a Carbo Pac PA20 column and a pulsed amperometric detector was employed to analyze monosaccharides of pectin. The procedure followed was in accordance with the method outlined by Wang et al. (2023). Pectin (10.00 ± 0.02 mg) was hydrolyzed using 4.00 mL of 2.00 mol/L trifluoroacetic acid (TFA) at 110 °C for 1 h. After dilution and filtration through a 0.22 μm filter, samples (10 μL) were injected into this system using a gradient elution program. Milli-Q water (A), 0.20 mol/L NaOH (B), and 1.00 mol/L NaAC (C) were used as eluents at a flow rate of 1.00 mL min^{-1}, meanwhile, the temperature of column was kept at 35 °C. In detail, the gradient elution program was as follows: 0–20 min: 91% A and 9% B, 20–20.1 min: 86% A, 9% B, and 5% C, 20.1–40 min: 71% A, 9 % B, and 20% C, 40–60 min: 100% B, 60–70.1 min: 91 % A and 9 % B. The contents of monosaccharides, namely, fucose (Fuc), rhamnose (Rha), arabinose (Ara), galactose (Gal), glucose (Glc), mannose (Man), and xylose (Xyl) were expressed as milligrams per gram of dry weight (mg/g AIR) (Wang et al., 2023).

2.9. Rheological properties

Rheological properties were performed with a rheometer (TA Instruments, New Castle, USA) equipped with parallel plates geometry (40 mm diameter, 1 mm gap). The dynamic testing was programmed in frequency sweep according to Liu, Shim, Shen, Wang, and Reaney (2017). Samples (5.00 ± 0.10 g) were settled between two parallel plates. Experimental flow curves were constructed through continuous shear at 25 °C, with a shear rate ranging from 0.01 to 100 s^{-1}. The frequency-dependent storage modulus (G′) and loss modulus (G″) were obtained at a constant temperature of 25 °C and a fixed strain of 1% followed by frequency sweep (0.01 logarithmic changed to 100 rad/s) tests (Liu et al., 2017) This method was carried out within the linear viscoelastic region to ensure the gel structures would not be damaged by the stress or the applied strain.

2.10. Texture properties

Texture profile analysis (TPA) mode was carried out to determine the texture properties using a texture analyzer (TA-XT2, Stable Micro System Ltd., Leicestershire, England) with a 36 mm diameter probe (P/36R) at room temperature. Parameters were as follows: the rate of pre-test, test, and post-test rates were 2, 1, and 1 mm/s, respectively. The holding time, trigger force and compression strain were 5 s, 5 g, and 70%, respectively.

2.11. Particle size and ζ-potential

Particle size distribution and ζ-Potential were measured by a laser particle size analyzer (S3500, Microtrac, USA) and a Zetasizer Nano ZS 3600 (Malvern Instruments GmbH, Herrenberg, Germany) at 25 °C, respectively.

2.12. Water holding capacity (WHC)

WHC was determined according to the centrifugation procedures. Samples (5.00 ± 0.10 g) were centrifugated for 10 min with 8000 r/min at 4 °C by a centrifuge (5804 R, Eppendorf (Shanghai) International Trade Co., Ltd, China) (Chen, Gan, Ji, Song, & Yin, 2019). WHC was calculated as equation (2)

$$\mathrm{WHC} = \frac{W_2 - W}{W_1 - W} \quad (2)$$

where, W was the weight of tube, g; W_1 was the initial total weight of samples and tubes, g; W_2 was the total weight of tubes and samples after centrifugation, g.

2.13. Low field nuclear magnetic resonance (LF-NMR)

The transverse relaxation time (T_2) was applied to analyze the moisture status, which was performed by an LF-NMR analyzer (MiniMR-60, Suzhou Niumag Analytical Instrument Corporation, Suzhou, China) equipped with a 0.5 T permanent magnet corresponding to a proton resonance frequency of 23.2 MHz at 32.00 ± 0.02 °C. Parameters for T_2 relaxation time measurements were settled as follows: TW (time waiting) = 2000 ms, TE (time echo) = 0.5 ms, NECH (number of echoes) = 12,000, and NS (number of scans) = 4. Logarithmic coordinates of raw data were used to construct the T_2 distribution curves with a multi-exponential model under the program of the MultiExp Inv Analysis (Suzhou Niumag Analytical Instrument Corporation, Suzhou, China) (Wang, Zhang, Bhandari, & Gao, 2016).

2.14. Fourier transform infrared spectroscopy (FT-IR)

The freeze-dried samples (1 mg) were mixed with KBr (100 mg), and then the resulting mixtures were ground and pressed into slices for FT-IR spectra further analysis. An FT-IR spectrophotometer (Tensor 27, Bruker, Germany) was performed with a resolution of 4 cm^{-1}, a cumulative scan of 64, and a wavelength range of 4000–400 cm^{-1} (Cui et al., 2023).

2.15. Scanning electron microscope (SEM)

The freeze-dried samples were placed into SEM specimen stub by a double-sided adhesive carbon tape. And then the samples were coated with thin gold under vacuum. The micromorphology was performed by a scanning electron microscope (SU8010, Hitachi Co., Tokyo, Japan) with an acceleration voltage of 10 kV. The magnification was of 250 × (Xie, Lyu, Wang, Bai, & Bi, 2024).

2.16. Statistical evaluation

All the experiments were performed at least in triplicate. The data was presented as the mean ± standard deviation (SD) and analyzed utilizing one-way analysis of variance (ANOVA) followed by LSD multiple comparison (SPSS.19.0 software, IBM Crop., Armonk NY USA). The significance level was established at $P < 0.05$. The figures were generated using Origin 9.0 software (Origin Lab Corporation, Northampton, USA).

3. Results and discussion

3.1. IDDSI

IDDSI provides the global standard and test methodology to evaluate food texture for people with dysphagia. As recommended, the fork pressure and spoon tilt tests were conducted to illustrate the feasibility of the peach pulp-SPI complex as dysphagia food. In this study, all samples were easily mashed with a fork when pressure was applied (Fig. 2a). A clear pattern was formed on the sample surface with no lumps and few particles. This illustrated that samples could be considered the dysphagia diet and marked as level 4-pureed/extremely thick foods or higher level. For the Cons sample, a visible pattern in the fork gap was found. Meanwhile, with the fork moving, this pattern was unclear and a short tail below the fork was formed, suggesting high mobility, which was closely correlated with rheological properties. However, with fork removal, no shape recovery was shown in Cons-SPI, YS-SPI and MR-SPI, indicating the decreased flow behavior of the complexes resulted from the addition of SPI. Due to its hydrophilic and hydrophobic groups, SPI acted as the amphiphilic polymer could both align with water and air. This interaction between SPI and polysaccharides in peach pulps favored the formation of viscoelastic network during heating, which contributed to the improved texture and stability for dysphagia-friendly foods that were easy to swallow and hold the shape (Li et al., 2021; Sow, Nicole Chong, Liao, & Yang, 2018). Additionally, the spoon tilt test was conducted to evaluate the stickiness and the cohesiveness (Fig. 2b), which could reflect texture properties of samples. When the spoons were tilted, Cons, Cons-SPI, YS, and MR stuck too tightly to slide off the spoons, revealing high stickiness and cohesiveness (Cheng, Zhang, Adhikari, & Islam, 2014). This required great tongue force to push the food into the pharynx. Therefore, Cons, Cons-SPI, YS, and MR samples would increase the risk of choking, which could not be classified into 5-minced/moist dysphagia diets. However, YS-SPI and MR-SPI held their shapes on the spoon and slid off the tilted spoon easily, with little food left on the spoon. Therefore, according to the IDDSI dysphagia diets, YS-SPI and MR-SPI should be categorized as level 5-minced/moist, owing to their appropriate swallowability without sticking to the tongue and pharynx. During heating processing, SPI unfolded to and interacted with substances in peach pulp, forming a viscoelastic layer and stabilizing YS-SPI and MR-SPI gels (Fu et al., 2023; Pycarelle, Bosmans, Nys, Brijs, & Delcour, 2020).

Based on the result of IDDSI, the characteristics of the prepared dysphagia diets varied from the properties of peach pulp. Moreover, the SPI-treated strategy significantly improved the fluidity, stickiness, and cohesiveness of peach pulp gels, which was beneficial for preparing dysphagia diets. Therefore, we further studied the characteristics of peach pulp-SPI gels based on the properties analysis of peach pulp. Furthermore, the interactions between peach pulp and SPI were also discussed.

3.2. DE-AIR, contents and sugar ratio of pectin fractions from peach pulps

For peach pulps, DE of AIR, contents and sugar ratio of pectin fractions were shown in Table 1. The highest DE (60.35%) was found in Cons-AIR, followed by MR-AIR (49.12%) and YS-AIR (43.67%). Thus, Con-AIR was HMP, while MR-AIR and YS-AIR were LMP. The low DE was always accompanied with the high viscosity and gel strength, because of the exceptional exposure of the carboxylic band and hydrogen bonding. This could contribute to texture degradation in fruit and vegetable and their products during processing.

Based on the solubilities and cross-linkages, pectin polymers were classified into three fractions, namely, WSP, loosely attached to the cell wall via non-covalent and non-ionic bonds, CSP, primarily composed of ionically cross-linked pectin, and NSP, predominantly connected to cell-wall polysaccharides by covalent ester bonds (Christiaens et al., 2016). As proven, pectin was the prominent polysaccharide in AIR from peach pulps, which ranged from 84.87 to 87.33 mg/g AIR. Among peach pulps, Cons showed the lowest WSP content (0.09 g/g AIR), YS performed the highest NSP content (0.29 g/g AIR), while MR had the highest total

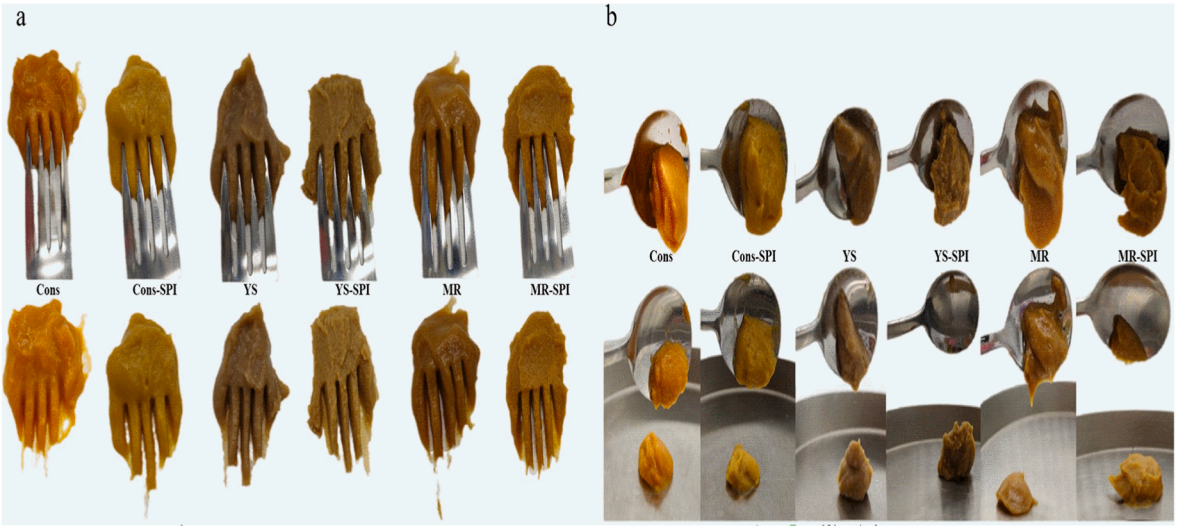

Fig. 2. The fork pressure test (a) and spoon tilt test (b) of peach pulp gels and peach pulp-SPI gels.

Table 1
Degree of esterification (DE) of alcohol insoluble residues (AIR) of peach pulps, sugar ratio and content of pectin fractions.

	DE (%)		Sugar ratio			Content (g/g AIR)
			A	B	C	
Cons	60.35 ± 1.73a	WSP	2.14 ± 0.01g	0.17 ± 0.01c	13.98 ± 0.21a	0.09 ± 0.01f
		CSP	5.53 ± 0.07d	0.12 ± 0.03d	5.32 ± 0.88f	0.49 ± 0.02a
		NSP	2.92 ± 0.01f	0.12 ± 0.02d	10.99 ± 0.27b	0.26 ± 0.03cd
YS	43.67 ± 2.54c	WSP	1.30 ± 0.03h	0.41 ± 0.01a	6.66 ± 0.13d	0.16 ± 0.01e
		CSP	2.17 ± 0.02g	0.26 ± 0.04b	8.93 ± 0.31c	0.40 ± 0.02b
		NSP	3.76 ± 0.08e	0.16 ± 0.04c	7.07 ± 0.05d	0.29 ± 0.02c
MR	49.12 ± 1.18b	WSP	8.56 ± 0.02a	0.04 ± 0.03f	6.00 ± 0.49e	0.13 ± 0.01ef
		CSP	7.37 ± 0.03c	0.08 ± 0.01e	4.57 ± 0.21g	0.51 ± 0.03a
		NSP	7.69 ± 0.02b	0.04 ± 0.04f	2.30 ± 0.28h	0.22 ± 0.02d

Note: Values are expressed as averages ± standard deviations (SD). Values followed by the different alphabets in the same column have a significantly difference ($p < 0.05$). WSP, water-soluble pectin; CSP, chelator-soluble pectin; NSP, Na_2CO_3-soluble pectin.

amount of pectin content (0.86 g/g AIR) and CSP content (0.51 g/g AIR).

Regarding the structure features, pectin typically consisted of homogalacturonan (HG), rhamnogalacturonan I (RG-I), and rhamnogalacturonan II (RG-II). These structure characters were closely contributed to the mechanical function of cell wall, which in turn reflected on the macro-texture properties of fruit and its products (Mao et al., 2019). Therefore, the sugar ratios were calculated. In detail, Sugar ratio A = GalA/(Fuc + Rha + Ara + Gal + Xyl), which was referred to linearity of pectin. Sugar ratio B = Rha/GalA, reflecting the proportion of RG-I backbone in pectin main chain. Sugar ratio C = (Ara + Gal)/Rha, indicating the number of branched sugar residues within RG-I region (Zhou, Bi, Chen, Wang, & Richel, 2021). Owing to the low GalA content and high rate of neutral sugar, Cons showed the low sugar ratio A and high sugar ratio C, demonstrating a low degree of linearity and high abundance of branching of RG-I. For YS, the low sugar ratio A and the notably high sugar ratio B illustrated the low linearity and major portion of the side chains from RG-I domain. The highest sugar ratios A ranged from 7.37 to 8.56 were found in MR, depicting the highest degree of linearity. However, sugar ratio B of MR varied from 0.04 to 0.08, which was relatively lower than that in Cons and YS. This indicated that MR had a relatively large HG region. For all pectin fractions, the lowest sugar ratio C was observed in pectin fraction of MR, verifying the lowest branched sugar residues within RG-I region. As reported, the longer pectin linearity and the lower branched sugar residues were favorable for gel formation (Renard & Thibault, 1993). Long-linearity pectin was preferred to form parallel or cross-linked junction zones with divalent ions (primarily Ca^{2+}) and create a tight three-dimensional network structure, which has been widely accepted as the "egg-box" model (Gawkowska, Cybulska, & Zdunek, 2018; Wang et al., 2018). In this sense, it was necessary to reveal physicochemical properties and texture formation of peach pulp-protein gel complexes based on the characteristics of peach pulp from different varieties.

3.3. Rheological properties

3.3.1. Apparent viscosity

Fig. 3a showed the apparent viscosity of peach pulps and peach pulp-SPI gels. With the increase in shear rate, the apparent viscosities of all the samples were significantly decreased, illustrating the pseudoplastic fluids properties with shear-thinning flow behavior. When subjected to high shear rate, the structures of peach pulp and peach pulp-SPI gel were damaged because of the disrupted molecular chains under the mechanical measurement (Wang, Sun, et al., 2024; Zhang, Chen, & Campanella, 2024). As the shear rate increased from 0.01 to 100 s^{-1}, the apparent viscosities of all samples rapidly decreased from 12,400 to 1400 Pa s to 6.88–0.55 Pa s.

For peach pulp gels, the highest viscosity was found in MR, while the lowest one was confirmed in Cons, which might vary from the hydrogen bond with different strengths in peach pulps. The low sugar content in Cons was not sufficient to enable CSP, that important to support the texture, to form a strong gel, which was reflected in its low apparent viscosity (Archut, Rolin, Drusch, & Kastner, 2023). When subjected to SPI addition, the apparent viscosity was significantly increased, probably due to the thickening of SPI (Jiang et al., 2020). Based on the molecular chain elongation and electrostatic attraction between SPI and substances in peach pulp (e.g., polysaccharides), the formed tight aggregation would also contribute to the strengthened apparent viscosity (Jones & McClements, 2008; Wang et al., 2024). Additionally, the interlink between SPI and polysaccharide also supported the formation of form the three-dimensional continuous network. As the post-heat drying processing, the molecular movement was accelerated, which could speed up the formation of the gel system (Wang et al., 2024; Zhang, Wang, Li, Li, & Qi, 2024). For peach pulp-SPI gels, the lowest apparent viscosity was observed in Cons-SPI, followed by MR-SPI and YS-SPI. AIR from MP and YS, considered as the LMP, exposed numerous free carboxyl groups and easily entangled with SPI through the strong electrostatic interaction, which contributed to the enhanced gel viscosity (Mao et al., 2023). These results were consistent with the spoon tilt

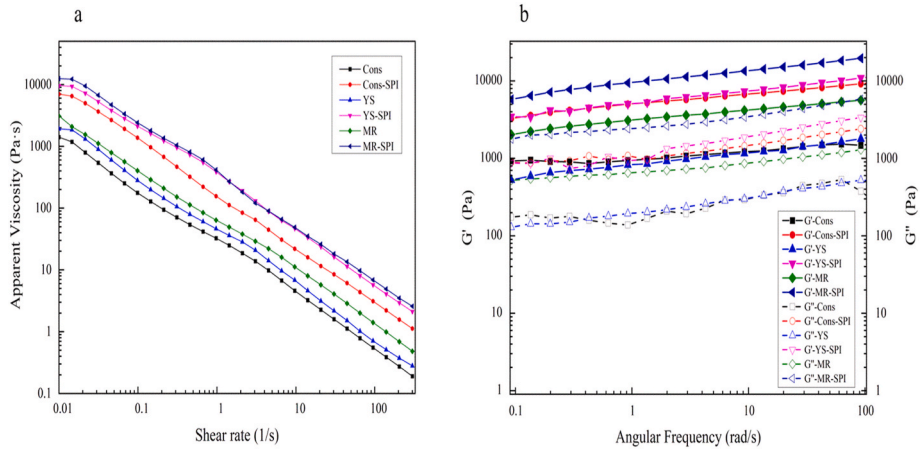

Fig. 3. The rheological properties of peach pulp gels and peach pulp-SPI gels, apparent viscosity (a), storage modulus (G′) and loss modulus (G″) (b).

test. When the shear rate was at 10 s^{-1}, apparent viscosity had a high correlation with oral cohesiveness perception, whereas, at 50 s^{-1}, it correlated with the effort of oral propulsion and at 10-50 s^{-1} that correlated with sensory appreciation (Laguna et al., 2021; Laguna, Manickam, Arancibia, & Tarrega, 2020). With the shear rate changes from 10 s^{-1} to 50 s^{-1}, the apparent viscosity of MR-SPI and YS-SPI showed a similar trend, which were corroborated well with the foods level in spoon tile test (Sharma, Pondicherry, & Duizer, 2022).

3.3.2. Dynamic rheological analysis

As shown in Fig. 3b, for peach pulps and peach pulp-SPI complexes, changes in storage modulus (G′) and loss modulus (G″) with angular frequency were depicted as elastic behavior and viscous behavior, respectively. Among all the samples, G′ was nearly one order of magnitude higher than G″ and remained constant over a wide range of 0.1–100 rad/s, indicating that samples could be considered as strong gel system (Ji, Xue, Zhang, Li, & Xue, 2017). With the increase in angular frequency, G′ and G″ were significantly increased.

Sucrose from peach pulp carried with equatorial-hydroxyl groups facilitated the aggregation of polysaccharides within pulp, which boosted the creation of dense and thick fibrillar junctions through the cross-linked hydrogen bonds. This process inflected on the enhanced gelation properties (Archut et al., 2023). For peach pulp gels, MR had notably higher G′ and G″, which could be explained by the improved stability of the network structure by the strong hydrogen bonds as SPI addition (Meng, Li, Yang, Wang, & Liu, 2024). Jiang et al. (2020) also described that hydrogen bonding played a major role in Mesona chinensis polysaccharide-whey protein isolate gel which displayed strong rheological properties. Compared with peach pulp gels, the pronounced increase in G′ and G″ was performed in all peach pulp-SPI gels. This outcoming suggested that SPI could improve the stability and the viscoelastic behavior of complexes through electrostatic interaction (Anvari et al., 2016). Additionally, the more hydrophobic and charged groups were exposed within SPI during the gel processing, which made it more available for inter-molecular interactions among polysaccharides from peach pulp alongside the increased G′ and G″ (Zhang et al., 2024). For the peach pulp-SPI gels, the highest G′ and G″ were observed in MR-SPI, which was consistent with the highest level in spoon tilt test. The highest G′ and G″ were attributed to the less branch chains and high linearity of MR pectin, which preferred to expose enough binding sites to bind with SPI (Han et al., 2017; Wang et al., 2018). Meanwhile, both Cons-SPI and YS-SPI performed the low G′ and G″, which did not show significant differences. This might account for the inhibited formation of insoluble complexes by electrostatic repulsion, covalent bonding or hydrophobic interaction of disulfide bonds between SPI and substances from peach pulp (Jiang et al., 2020). Obviously, the value differences in G′ and G″ among peach pulp-SPI gels were significantly smaller than that among peach pulp gels. It was reasonable to conclude that the elastic solid-like behavior of peach pulp-SPI gels depended on not only the properties of peach pulps but also the features of the complexes. Additionally, the friction and entanglement between SPI particles and cell wall polymers were varied from the contents and properties of AIR and pectin, which might contribute to the different covalent bonding or electrostatic interaction (Jiang et al., 2020).

3.4. Texture

The texture properties were shown in Fig. 4. In peach pulp gels, MR showed the highest hardness (15.79 g), springiness (0.75) and chewiness (8.15), followed by YS and Cons. The long linearity and low branched in pectin polymers from MR contributed to the strong texture properties. Additionally, the high cohesiveness of MR might relate to the numerous hydroxyl groups and free carboxyl groups. No significant differences in adhesiveness were found among Cons, YS, and MR. After compounding with SPI, the texture properties of peach pulp gels were significantly altered, corresponding to the formation of complexes. This improvement also could be explained by the SPI aggregation induced by the electrostatic interaction between charged protein molecules, which was deeply promoted by Ca^{2+} (Gawkowska et al., 2018; Wang et al., 2018). As for peach pulp-SPI complexes, MR-SPI had the highest hardness (79.65 g), followed by YS-SPI and Cons-SPI. However, the most pronounced

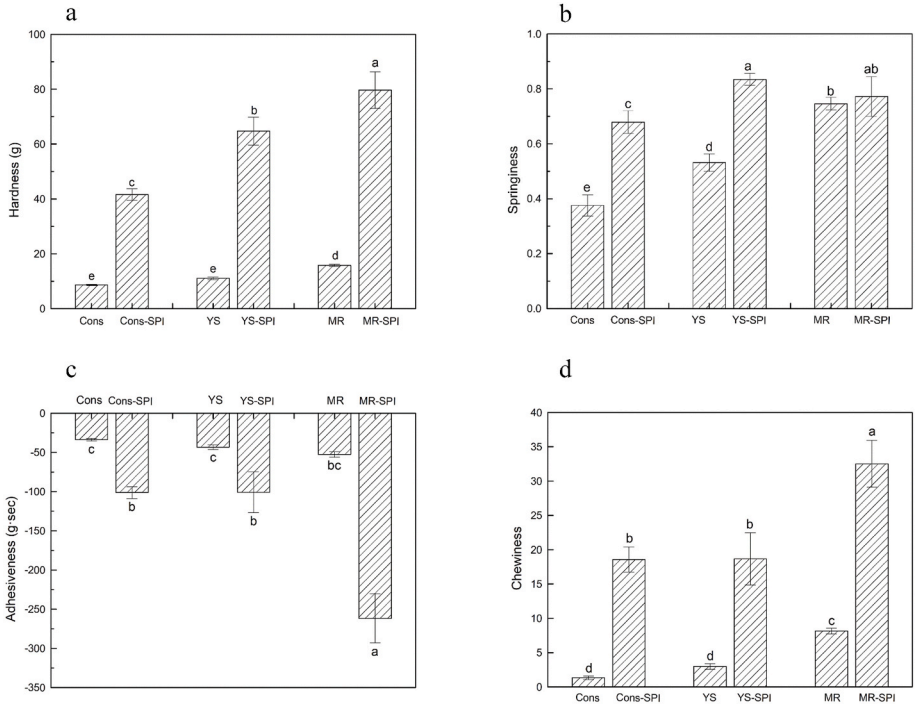

Fig. 4. Textural properties of peach pulp gels and peach pulp-SPI gels, hardness(a), springiness (b), adhesiveness (c), chewiness (d).
Note: Different lowercase letters indicate significant differences among treatments ($p < 0.05$).

increase ratio of hardness (484.01%) was found in YS-SPI (Fig. 4a). AIR from YS with low DE value exposed numerous binding sites to capture positive charge particles, contributing to the strong binding strength and facilitate the formation of complexes (Wang, Munk, Skibsted, & Ahrné, 2022). The highest springiness (0.83) was observed in YS-SPI, followed by MR-SPI (0.77) (Fig. 4b), which were consistent with their high G′ value. The lowest springiness (0.68) was found in Cons-SPI, which also had a low G′ value. Concerning adhesiveness, the highest value (261.65 g s) was also confirmed in MR-SPI. No statistical significance was achieved in adhesiveness between YS-SPI and Cons-SPI (Fig. 4c). A similar result was observed in chewiness, MR-SPI performed the highest chewiness (32.53), followed by YS-SPI and Cons-SPI (Fig. 4d). This observation could be explained by SPI addition and the properties of peach pulp from different varieties. There might be two reasonable explanations for the improved texture properties. First, following SPI addition, the reduced overlap and spatial repulsion within the matrix (namely, the excluded volume effect) accelerated the effective concentration and the electrostatic interaction between peach pulp and SPI (Wang et al., 2024; Wang, Jiang, et al., 2024). In addition, the formation of protein self-aggregates and protein-polysaccharides complex with dense structure might be further facilitated by post-heating processing, which also contributed to the enhanced texture properties (Guo et al., 2018).

3.5. Particle size

A leftward shift of distribution peaks signified a reduction in particle size, meanwhile, the diminished peak width indicated a uniform size distribution, while, D50 performed as the mean diameter (Fig. 5). For peach pulps, the biggest mean diameter was observed in MR, indicating the largest particle size. This phenomenon might lead to the increased interparticle friction between particles, which was consistent with the high apparent viscosity, G′ and G″. While the smallest particle size was obtained in YS.

In comparison with peach pulp, the peaks in peach pulp-SPI were significantly left-shift except MR-SPI. The results indicated the reduction in particle size of Cons-SPI and YS-SPI, owing to strong interaction between SPI and polysaccharides of peach pulp. Additionally, the declined mean diameter in peach pulp-SPI might also depend on the reduced protein self-aggregation resulting from polysaccharide blocking binding sites of unfolded SPI. Our observation aligned with the result of Yi, Gan, Wen, Fan, and Wu (2021), who reported a reduction in particle size of pea protein following incorporation with pectin (Yi et al., 2021). Furthermore, compared with peach pulp gels, the particle size of peach pulp-SPI gels became more uniform according to the alterations in peak width. Cons-SPI gel exhibited abundance of small particles, while YS-SPI and MR-SPI achieved an increased proportion of large particles, while, the large article was usually associated with improved cohesiveness. This result was also corroborated by the spoon test and fork test. The rightmost peak point, illustrating the biggest mean diameter, was depicted in MR-SPI. And a significant difference in D50 was solely observed between MR-SPI and MR, indicating the development of new complexes composed of MR pulps and SPI particles through electrostatic interaction (Jones, Decker, & McClements, 2009).

3.6. ζ-potential

The magnitude of ζ-potential was performed to evaluate the stability of samples and explain the intensity of electrostatic attraction or repulsion between adjacent particles in a colloidal system (Fig. 6) (Ma et al., 2019). Among all the peach pulp samples, based on the high charges of LMP from YS, the highest value of ζ-potential (−27.57 mV) was found, implying its instability, which easily interacted with SPI (Wang et al., 2022). No significant differences in ζ-potential were observed between Cons and MR, indicating similar stability. SPI, carrying positive charges, could neutralize the partial negative charges from peach pulps (e.g., pectin polysaccharides) (Ma et al., 2019), contributing to the decreased values of ζ-potential in peach pulp-SPI gels. The mixing of peach pulp and SPI resulted in a ζ-potential intermediate between the two polyelectrolytes (Zhang, Huang, Geng, Teng, & Xiao, 2021). The highest ζ-potential (−23.55 mV) was shown in YS-SPI, owing to the numerous free carboxylic groups of LMP from YS-AIR and the strong interaction between SPI and YS pulp (Pillai, Guldiken, & Nickerson, 2021). Additionally, compared with YS, MR and Cons, the values of ζ-potential in YS-SPI, MR-SPI and Cons-SPI decreased by 14.58%, 9.53% and 9.43%, respectively.

3.7. WHC

As shown in Fig. 7, WHC values were varied between peach pulp gels and peach pulp-SPI gels. Among peach pulp gels, MR performed the highest WHC (80.80%), which was in line with the strong hydrogen bonds between water and pectin resulting from the high content and the high linearity of pectin. While, pectin (from Cons) as HMP could not form the strong gel structure under neutral environment (Roque et al., 2022), which contributed to the lowest WHC (47.33%). When subjected to SPI addition, the WHC of peach pulp-SPI gels was significantly

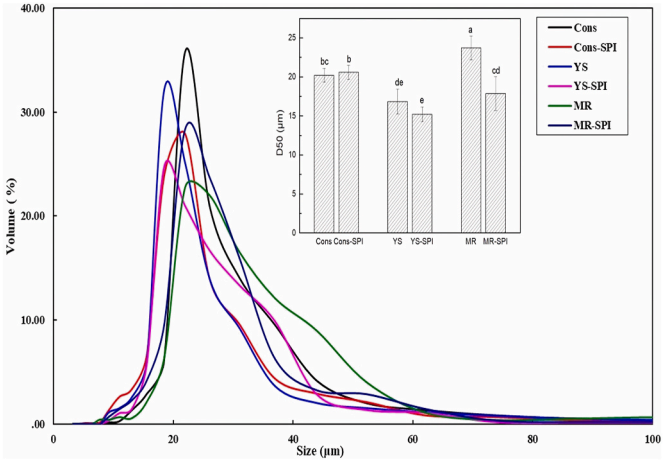

Fig. 5. Particle size distribution of peach pulp gels and peach pulp-SPI gels.
Note: The insert picture is the D50 of the peach pulp gels and peach pulp-SPI gels. Different lowercase letters indicate significant differences among treatments ($p < 0.05$).

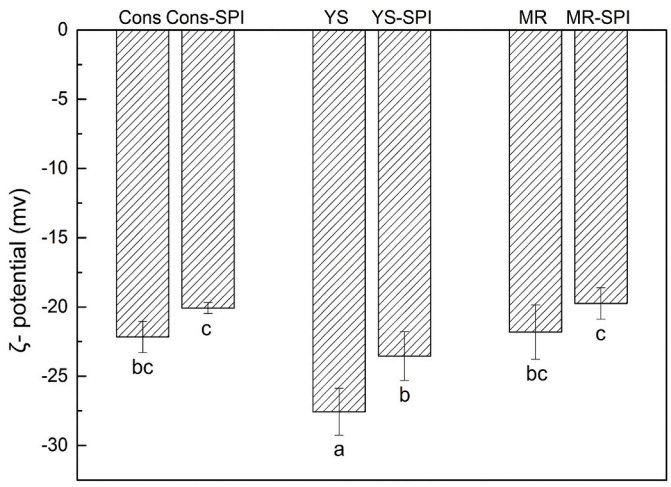

Fig. 6. ζ-Potential of peach pulp gels and peach pulp-SPI gels.
Note: Different lowercase letters indicate significant differences among treatments ($p < 0.05$).

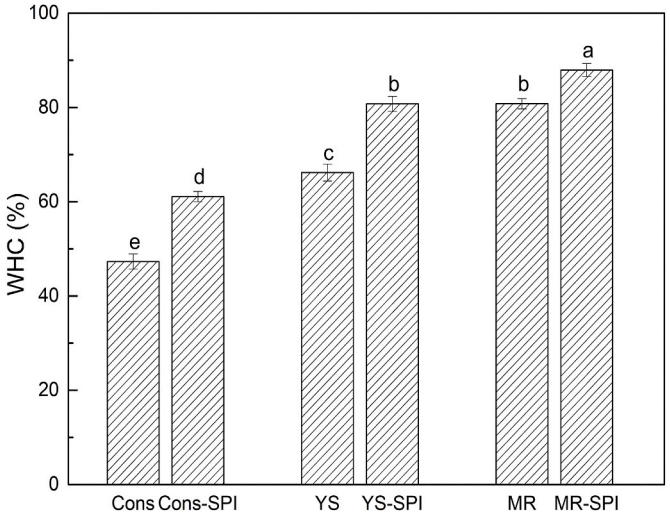

Fig. 7. Water holding capacity (WHC) of peach pulp gels and peach pulp-SPI gels.
Note: Different lowercase letters indicate significant differences among treatments ($p < 0.05$).

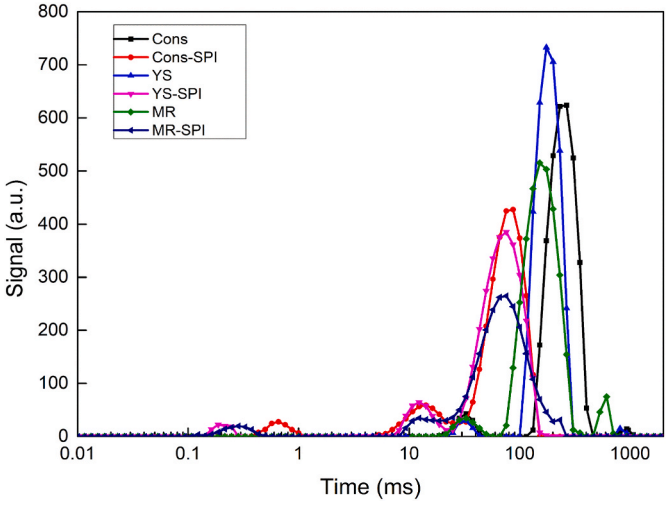

Fig. 8. The transverse relaxation (T_2) curves of peach pulp gels and peach pulp-SPI gels.

improved, with the increased rates of 29.11%, 22.01%, and 8.84% for Cons-SPI, YS-SPI, and MR-SPI, respectively. These outcomes could be explained by the differential entrapment of moisture in peach pulp-SPI complexes with various properties (Jiang et al., 2020). During the gels processing, substances in peach pulp and SPI filled into the gap of gels to form a dense network structure. Meanwhile, SPI molecules denatured and reorganized into this network that trapped water molecules during thermal gelation (Fu et al., 2023; Xue et al., 2023). It should be noted that the enhanced WHC was associated with the strong ability to capture the moisture molecules, which supported the softness of dysphagia food. Additionally, foods with high WHC were less likely to break down into crumbs during chewing, which could significantly reduce the risk of food particles entering the trachea during swallowing. Therefore, this high WHC was vital for preventing aspiration in patients with swallowing difficulties (Fu et al., 2023; Xue et al., 2023). Among the complex gels, the numerous hydroxylate groups and carboxylate groups in MR could easily form hydrogen bonds with water and hydrophilic groups in SPI and promote the formation of peach pulp-SPI complexes (Sun, Li, Xu, & Zhou, 2011), accompanied with the highest WHC (87.94%). Furthermore, the complex gel networks, characterized by strong internal bonds, exhibited the stable and dense texture, which was reflected on the highest WHC at macro-level (Wang et al., 2020).

3.8. LF-NMR

The water states in peach pulp gels and complex gels were characterized by spin-spin relaxation time (T_2) (Fig. 8). The shortest relaxation time (T_{21}) ranging from 0.1 to 1 ms, was assigned to bound water. This water was captured in cell wall based on a chemical exchange effect resulting from the rapid exchange of protons between water and hydroxyl groups from the rigid cell wall polysaccharides (such as pectin, cellulose, and hemicellulose) (Cheng et al., 2014). The intermediate relaxation time (T_{22}), ranging from 5.33 to 351 ms, was attributed to immobilized water, which presented in the cytoplasm accompanied with high viscosity. The longest relaxation time (T_{23}), ranging from 533 to 1000 ms, was assigned to free water located within the vacuole, which was due to the slowest chemical exchange between water and sugars or other substances with small molecular weight. For peach pulp gels, the three water fractions, in which immobilized water was dominant, could be obviously distinguished. T_{22} was decreased in YS and MR compared with Cons. Generally, the lower relaxation direction in T_{22} suggested the decreased mobility in water, owing to the dense gel structure. Especially, polysaccharides and carboxylate in LMP could easily form dense structure and capture water through Ca^{2+} bridge. Alternatively, LMP could form gel structure and lock water according to the "egg-box model" under heating conditions (Gawkowska et al., 2018). This result was also supported by the results of WHC. Only small proportion of free water was found in peach pulp gels. The most obvious presence of free water was observed in MR, indicating a higher degree of water mobility. However, no significant signal of bound water was completely found in peach pulp gels.

When SPI was applied to peach pulp, the water status of the samples was significantly changed. Compared with peach pulp, the signal of relaxation time was sizably declined in peach pulp-SPI complexes. These differences could be explained by the various polysaccharides of peach pulp matric, which contributed to the distinct interaction between water and SPI or other cellular components (Peters, Vergeldt, Boom, & van der Goot, 2017). SPI exposed numerous hydrophobic groups inside molecules strongly bonded with polysaccharides through hydrophobic interactions to form a polysaccharides-SPI network structure, which might enable free water transfer into immobilized water (Fu et al., 2023). Moreover, as SPI addition, the relaxation time in all peach pulp-SPI complexes was gradually moved to the higher relaxation time, indicating the strong water binding capacity in complexes. When subjected to the thermal gelation, SPI represented a structural unfolding state accompanied by more hydrophobic groups and easily formed the salt bridges with metal ions (e.g. Ca^{2+}), which could reduce the moisture's mobility (Xue et al., 2023). Notably, free water was not detected in peach pulp-SPI gels, suggesting the transfer between free water and immobilized water during SPI swelling and peach pulp-SPI complexes formation (Luo et al., 2020). This decrease in free water could slow down microbial growth and extend the shelf life of the peach pulp-SPI complex gels (Kamal et al., 2019). T_2 results showed that immobilized water was the dominant water in peach pulp-SPI complexes, which was similar with T_2 in Cons, YS and MR. This indicated the strong link among SPI, peach pulp and water. Only a small signal of bound water appeared in peach pulp-SPI gels, but not in peach pulp gels. This was because bound water was only trapped within large molecules by strong hydroxyl groups (Çakır & Foegeding, 2011). T_{21} was shorter in YS-SPI and MR-SPI than in Cons-SPI, suggesting that most of the water in YS-SPI and MR-SPI was bound with carbohydrates within the dense microstructure. Moreover, this compact structure was beneficial for dysphagia diet.

3.9. FT-IR

As shown in Fig. 9, the peaks ranged from 3700 to 3000 cm^{-1} were

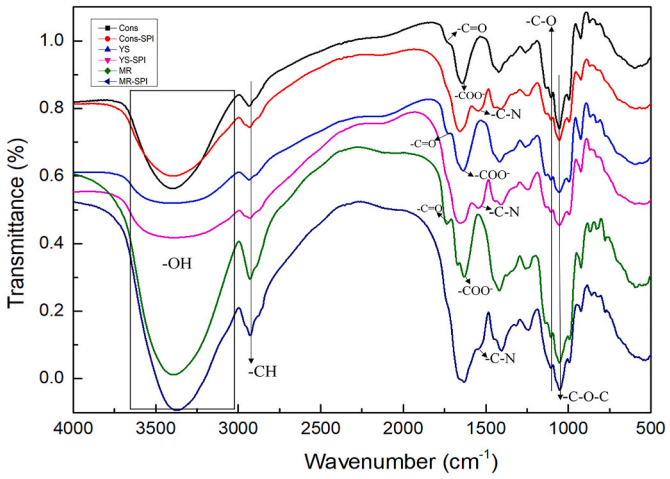

Fig. 9. FT-IR spectra of peach pulp gels and peach pulp-SPI gels.

mainly related to hydroxyl group (O–H) stretching vibrations. The peak around 2930 cm^{-1} was contributed to the stretching vibration of the carbon-hydrogen bond (-CH). The band between 2950 and 2750 cm^{-1} corresponded to the stretching of methyl esters group of galacturonic acid (O–CH_3) (Yu, Li, Hu, Wang, & Bi, 2023). The characteristic bands at 1740 cm^{-1} and 1630 cm^{-1} were attributed to the stretching of ester carbonyl (C═O) groups and the stretching of carboxylic band (COO^-), respectively, which were both related to DE of cell wall polymers (Ran & Yang, 2022). The peak around 1417 cm^{-1} was assigned to symmetric stretching of COO^- (Yan et al., 2023). For peach pulp gels, the intensity of the absorption band around 3390 cm^{-1} (O–H) was significantly varied in Cons, YS and MR (Table S1). The strongest intensity of O–H absorption peak (3700 - 3000 cm^{-1}) was found in MR, followed by Cons. The wide and flat absorption peak at 3693 - 3000 cm^{-1} (O–H) was observed in YS. The strong intense absorptions at 2929 cm^{-1} (CH) and 1631 cm^{-1} (COO^-) were found in MR. Meanwhile, the sharp peak at 1053 cm^{-1} corresponding to C–O–C was both obtained in Cons and MR, associating with Arabinose (Synytsya, 2003). The bands between 2950 and 2750 cm^{-1} (O–CH_3) were significantly different among Cons, YS, and MR, corresponding to the distinct DE of cell wall polymers. Additionally, these differences in the tense and width of peaks around 1740 cm^{-1} and 1630 cm^{-1} indicating DE of cell wall polymers could be attributed to the distinct skeletal modes of peach pulp gels with different varieties.

When subjected to SPI addition, significant right-shift was obtained in the O–H groups (3390 cm^{-1}), suggesting the formation of strong intramolecular and intermolecular hydrogen bonding in peach pulp-SPI complexes (Han, Zhang, Fei, Xu, & Zhou, 2009). Compared with peach pulp gels, namely, Cons, YS and MR, the carboxyl absorption bands in peach pulp-SPI gels were significantly left shifted, which were increased from 1643, 1637, and 1631 to 1656, 1651, and 1639 cm^{-1}, respectively. Moreover, the carboxyl absorption with broader peaks (1706 - 1558 cm^{-1}) was observed in peach pulp-SPI gels, highlighting the stronger electrostatic interaction between SPI and COO^- group of peach pulps. The presence of electrostatic interaction of polysaccharides-protein was also described by He et al. (2021). Furthermore, the intense peaks of C–N (1540 cm^{-1}) were found in peach pulp-SPI gels, while not observed in peach pulp gels, confirming the formation of new complexes. Additionally, the absence of C═O peaks (1645 cm^{-1}) in peach pulp-SPI gels might be attributed to the collapsed chemical group of cell wall disordered by SPI addition (Gu et al., 2010). The weakened absorptions in the region of 1540–1180 cm^{-1} were observed in peach pulp-SPI gels, illustrating that SPI might attach to the substances (e.g., cell wall polymers) of peach pulp. This result was also confirmed in the formation of curcumin-pea protein isolate complex (Guo et al., 2021). Additionally, the formation of a new complex was also identified by the changes in absorption bands around 1100 cm^{-1} and 1050 cm^{-1}, resulted from the stretching vibration of C–C, C–O and the bending vibration of C–O–C (referred to "saccharide"). In addition, MR-SPI showed the widest and the most intense absorption around 3390 cm^{-1} assigned to hydroxyl group, which was consistent with the strong cohesiveness from IDDIS result.

3.10. Microstructure

The structures of peach pulp gels and peach pulp-SPI gels at the submicron level were obtained by SEM (Fig. 10a). For Cons, the loose and big pores were observed and illustrated the damaged cell structure during grinding process. Additionally, no significant gel network was formed for Cons, probably because of the low linearity and high degree of branching of cell polymers. A tight structure with varied porous was found in YS. Meanwhile, MR revealed a dense and homogeneous multilayer skeleton structure, which was beneficial for capturing moisture molecules within its network. Furthermore, MR-AIR with low DE and pectin with high linearity could facilitate the formation of dense and regular network structure. Taken together, the mesh-like network with varied porous structures of peach pulp gels could be characterized by the stacking of cell wall polysaccharides through hydrogen bonding and electrostatic interactions.

Cons-SPI gels had numerous large pores and the separated big SPI particles were observed on their cell wall polysaccharide layer. The relatively limited quantity of free carboxyl groups in Cons could not provide enough binding sites for SPI, contributing to the weak interaction accompanied with the loose microstructure. For YS-SPI, the abundant hydrogen bonds with exposed binding sites from YS could be tightly attached with the spherical proteins through electrostatic repulsion. However, under the acidic environment induced by YS pulp, the excess SPI could exhibit self-aggregation, resulting in big porous and homogenous structure. In addition, the aggregation of small particle size in YS-SPI (Fig. 5) might also contribute to the dense network (Sow et al., 2018). MR-SPI performed a dense and continuous gel-like network structure, suggesting the formation of electrostatic complexation as the consequence of the cross-linking between spherical protein particles and peach pulp flakes (He et al., 2021). This result agreed with the strengthened texture properties (Fig. 4a–d). Therefore, this dense micro-structure combined with this strengthened macro-texture could resist the deformation and prevent choking while chewing in mouth (Li et al., 2021). Furthermore, as the low DE and high GalA content, cell wall polymers in MR provided a number of available reactive sites for complexation with SPI (Warnakulasuriya et al., 2018).

Based on the results of rheology, WHC, LF-NMR, FTIR and SEM, the schematic model of effect of SPI on peach pulp was proposed in Fig. 10b. In the acidic environment induced by peach pulp, SPI, carrying positively charged particles, attracted with cell wall polymers (e.g., polysaccharides) from peach pulp with typically negatively charged through electrostatic interaction. As SPI swelled and its secondary structure unfolded, polysaccharides in peach pulp became entangled with SPI accompanied by the exposure of hydrophobic groups and sulfhydryl groups. During post-heat processing, a promoted binding effect between polysaccharides and proteins would be explained by the changes in conformation and structure of peach pulp-SPI complexes, in which a core-shell structure was formed and the protein as the core and polysaccharides entangled outside (Jiang et al., 2020; van de Velde, de Hoog, Oosterveld, & Tromp, 2015). This structure was a relatively stable three-dimensional gel network. When the positive charges (from polysaccharides) aligned with the negative charges (from protein particles), their binding interaction was maximized. However, when there was limited quantity of polysaccharide, some of protein particles were buried in peach pulp-SPI gels network without binding with polysaccharide and formed large but loose aggregates, like Cons-SPI. Conversely, the excessive polysaccharides provided by fruit gel would hinder self-aggregation due to electrostatic repulsion (Mao et al., 2023).

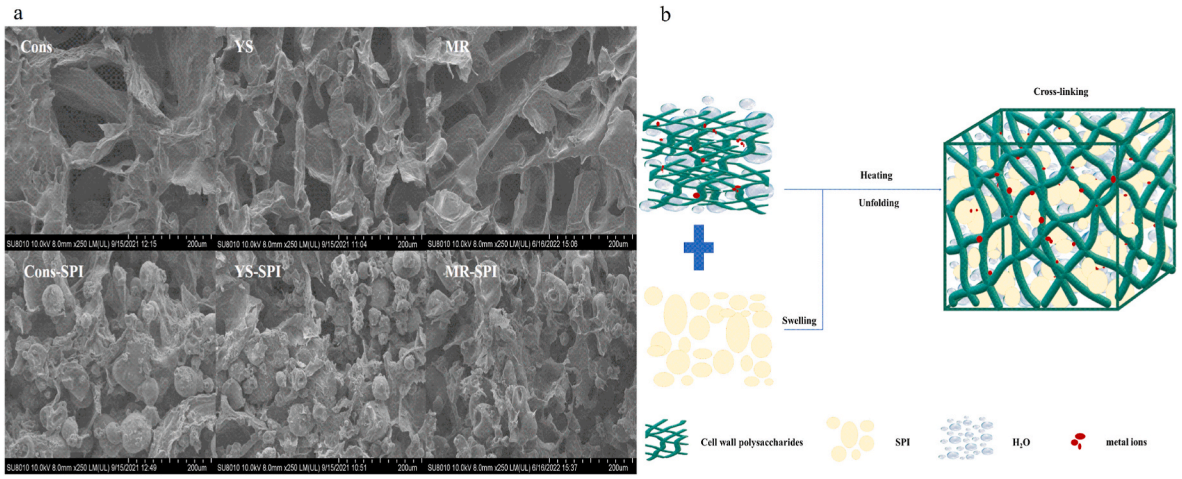

Fig. 10. Scanning electron microscopy (SEM) pictures of peach pulp gels and peach pulp-SPI gels (a). A model for peach pulp - soy protein isolate (SPI) complex (b).

Therefore, SPI denaturation and self-aggregation were preferred to support the formation of small peach pulp-SPI aggregations, like YS-SPI.

4. Conclusion

In this study, peach pulp-SPI complex, with SPI incorporated into various peach pulps as natural polysaccharide carriers, served as a model system for dysphagia food. Based on their low cohesiveness in the spoon tilt test, peach pulp gels were failure to be classified as level 5 in the IDDSI test. The addition of SPI enabled the formation of dense and regular microstructures within peach pulp-SPI complex, accompanied by improved rheology, textural properties, and WHC. These results could be confirmed by the strengthened hydrogen bonds and electrostatic interactions from FTIR results. Furthermore, when subjected to SPI addition, peach pulp-SPI complexes (especially for YS-SPI and MR-SPI) exhibited dense network structures, which were aligned with IDDSI testing for level 5 minced/moist dysphagia foods. Since AIR with low DE carried numerous active sites, like hydroxyl group and free carboxyl groups, it was easy to form peach pulp-SPI complexes. Moreover, pectin from peach pulp with high linearity and few branches facilitated the electrostatic interactions between pectin and SPI, which contributed to the strengthened texture properties. Specially for MR-SPI, the improved cohesiveness might be associated with the large particles. Additionally, apparent viscosity of MR-SPI at 10 s^{-1} was demonstrated a strong correlation with spoon tilt test of IDDSI, whereas G′ was a significant association with the springiness of TPA test. These findings suggested MR might be the optimal choice to form gel food for people with swallowing problem. This work might provide valuable insights on the development of dysphagia-friendly diets in which natural fruit pulps as the food matrices.

CRediT authorship contribution statement

Jin Xie: Writing – original draft, Visualization, Methodology, Investigation, Data curation, Conceptualization. **Jinfeng Bi:** Supervision, Project administration, Funding acquisition. **Jacquet Nicolas:** Writing – review & editing. **Blecker Christophe:** Writing – review & editing, Formal analysis. **Fengzhao Wang:** Writing – review & editing. **Jian Lyu:** Writing – review & editing, Supervision, Project administration.

Declaration of competing interest

The authors declared that they have no conflicts of interest to this work. We declare that we do not have any commercial or associative interest that represents a conflict of interest in connection with the work submitted.

Data availability

Data will be made available on request.

Acknowledgments

The research was supported by China Agriculture Research System (CARS-30-5-02).

Appendix A. Supplementary data

Supplementary data to this article can be found online at https://doi.org/10.1016/j.foodhyd.2024.110130.

References

Anvari, M., Tabarsa, M., Cao, R., You, S., Joyner, H. S., Behnam, S., et al. (2016). Compositional characterization and rheological properties of an anionic gum from Alyssum homolocarpum seeds. *Food Hydrocolloids, 52*, 766–773.

Archut, A., Rolin, C., Drusch, S., & Kastner, H. (2023). Interaction of sugar beet pectin and pea protein: Impact of neutral sugar side chains and acetyl groups. *Food Hydrocolloids, 138*, Article 108454.

Çakır, E., & Foegeding, E. A. (2011). Combining protein micro-phase separation and protein–polysaccharide segregative phase separation to produce gel structures. *Food Hydrocolloids, 25*(6), 1538–1546.

Chen, H., Gan, J., Ji, A. G., Song, S. L., & Yin, L. J. (2019). Development of double network gels based on soy protein isolate and sugar beet pectin induced by thermal treatment and laccase catalysis. *Food Chemistry, 292*, 188–196.

Cheng, X.-f., Zhang, M., Adhikari, B., & Islam, M. N. (2014). Effect of power ultrasound and pulsed vacuum treatments on the dehydration kinetics, distribution, and status of water in osmotically dehydrated strawberry: A combined NMR and DSC study. *Food and Bioprocess Technology, 7*(10), 2782–2792.

Christiaens, S., Van Buggenhout, S., Houben, K., Jamsazzadeh Kermani, Z., Moelants, K. R., Ngouemazong, E. D., et al. (2016). Process-structure-function relations of pectin in food. *Critical Reviews in Food Science and Nutrition, 56*(6), 1021–1042.

Cui, J., Zhang, L., Wang, J., Zhao, S., Zhao, C., Liu, D., et al. (2023). Study on the relationship between primary structure/spatial conformation and gel properties of pectins from different varieties. *Food Hydrocolloids, 144*, Article 109055.

Fu, H., Li, J., Yang, X., Swallah, M. S., Gong, H., Ji, L., et al. (2023). The heated-induced gelation of soy protein isolate at subunit level: Exploring the impacts of α and α′ subunits on SPI gelation based on natural hybrid breeding varieties. *Food Hydrocolloids, 134*, Article 108008.

Gawkowska, D., Cybulska, J., & Zdunek, A. (2018). Structure-related gelling of pectins and linking with other natural compounds: A review. *Polymers, 10*(7), 762.

Gu, F.-L., Kim, J. M., Abbas, S., Zhang, X.-M., Xia, S.-Q., & Chen, Z.-X. (2010). Structure and antioxidant activity of high molecular weight Maillard reaction products from casein–glucose. *Food Chemistry, 120*(2), 505–511.

Guo, Q., Bayram, I., Zhang, W., Su, J., Shu, X., Yuan, F., et al. (2021). Fabrication and characterization of curcumin-loaded pea protein isolate-surfactant complexes at neutral pH. *Food Hydrocolloids, 111*, Article 106214.

Guo, Y., Zhang, X., Hao, W., Xie, Y., Chen, L., Li, Z., et al. (2018). Nano-bacterial cellulose/soy protein isolate complex gel as fat substitutes in ice cream model. *Carbohydrate Polymers, 198*, 620–630.
Han, W., Meng, Y., Hu, C., Dong, G., Qu, Y., Deng, H., et al. (2017). Mathematical model of Ca^{2+} concentration, pH, pectin concentration and soluble solids (sucrose) on the gelation of low methoxyl pectin. *Food Hydrocolloids, 66*, 37–48.
Han, M., Zhang, Y., Fei, Y., Xu, X., & Zhou, G. (2009). Effect of microbial transglutaminase on NMR relaxometry and microstructure of pork myofibrillar protein gel. *European Food Research and Technology, 228*(4), 665–670.
He, Z., Liu, C., Zhao, J., Li, W., & Wang, Y. (2021). Physicochemical properties of a ginkgo seed protein-pectin composite gel. *Food Hydrocolloids, 118*, Article 106781.
IDDSI. (2019). IDDSI framework. Retrieved from https://iddsi.org/Framework. (Accessed 29 November 2023).
Ji, L., Xue, Y., Zhang, T., Li, Z., & Xue, C. (2017). The effects of microwave processing on the structure and various quality parameters of Alaska pollock surimi protein-polysaccharide gels. *Food Hydrocolloids, 63*, 77–84.
Jiang, L., Ren, Y., Xiao, Y., Liu, S., Zhang, J., Yu, Q., et al. (2020). Effects of Mesona chinensis polysaccharide on the thermostability, gelling properties, and molecular forces of whey protein isolate gels. *Carbohydrate Polymers, 242*, Article 116424.
Jones, O. G., Decker, E. A., & McClements, D. J. (2009). Formation of biopolymer particles by thermal treatment of beta-lactoglobulin-pectin complexes. *Food Hydrocolloids, 23*(5), 1312–1321.
Jones, O. G., Lesmes, U., Dubin, P., & McClements, D. J. (2010). Effect of polysaccharide charge on formation and properties of biopolymer nanoparticles created by heat treatment of β-lactoglobulin–pectin complexes. *Food Hydrocolloids, 24*(4), 374–383.
Jones, O. G., & McClements, D. J. (2008). Stability of biopolymer particles formed by heat treatment of β-lactoglobulin/Beet pectin electrostatic complexes. *Food Biophysics, 3*(2), 191–197.
Kamal, T., Cheng, S., Khan, I. A., Nawab, K., Zhang, T., Song, Y., et al. (2019). Potential uses of LF-NMR and MRI in the study of water dynamics and quality measurement of fruits and vegetables. *Journal of Food Processing and Preservation, 43*(11), Article e14202.
Laguna, L., Manickam, I., Arancibia, C., & Tarrega, A. (2020). Viscosity decay of hydrocolloids under oral conditions. *Food Research International, 136*, Article 109300.
Laguna, L., Rizo, A., Pineda, D., Pérez, S., Gamero, A., & Tárrega, A. (2021). Food matrix impact on oral structure breakdown and sandiness perception of semisolid systems including resistant starch. *Food Hydrocolloids, 112*, Article 106376.
Li, J., Yang, X., Swallah, M. S., Fu, H., Ji, L., Meng, X., et al. (2021). Soy protein isolate: An overview on foaming properties and air–liquid interface. *International Journal of Food Science and Technology, 57*(1), 188–200.
Liu, Z., Chen, X., Dai, Q., Xu, D., Hu, L., Li, H., et al. (2023). Pea protein-xanthan gum interaction driving the development of 3D printed dysphagia diet. *Food Hydrocolloids, 139*, Article 108497.
Liu, J., Shim, Y. Y., Shen, J., Wang, Y., & Reaney, M. J. T. (2017). Whey protein isolate and flaxseed (Linum usitatissimum L.) gum electrostatic coacervates: Turbidity and rheology. *Food Hydrocolloids, 64*, 18–27.
Luo, H., Guo, C., Lin, L., Si, Y., Gao, X., Xu, D., et al. (2020). Combined use of rheology, LF-NMR, and MRI for characterizing the gel properties of hairtail surimi with potato starch. *Food and Bioprocess Technology, 13*(4), 637–647.
Ma, X., Hou, F., Zhao, H., Wang, D., Chen, W., Miao, S., et al. (2020). Conjugation of soy protein isolate (SPI) with pectin by ultrasound treatment. *Food Hydrocolloids, 108*, Article 106056.
Ma, X., Yan, T., Hou, F., Chen, W., Miao, S., & Liu, D. (2019). Formation of soy protein isolate (SPI)-citrus pectin (CP) electrostatic complexes under a high-intensity ultrasonic field: Linking the enhanced emulsifying properties to physicochemical and structural properties. *Ultrasonics Sonochemistry, 59*, Article 104748.
Mao, Y., Huang, M., Bi, J., Sun, D., Li, H., & Yang, H. (2023). Effects of kappa-carrageenan on egg white ovalbumin for enhancing the gelation and rheological properties via electrostatic interactions. *Food Hydrocolloids, 134*, Article 108031.
Mao, Y., Lei, R., Ryan, J., Arrutia Rodriguez, F., Rastall, B., Chatzifragkou, A., et al. (2019). Understanding the influence of processing conditions on the extraction of rhamnogalacturonan-I "hairy" pectin from sugar beet pulp. *Food Chemistry X, 2*, Article 100026.
Meng, F., Li, J., Yang, C., Wang, M., & Liu, X. (2024). Rheological and tribological properties of high internal phase emulsions stabilized by pH-induced soy protein isolate-carrageenan complex coacervates. *Food Hydrocolloids, 146*, Article 109191.
Milošević, M. M., & Antov, M. G. (2022). Pectin from butternut squash (Cucurbita moschata) – the effect of enzyme-assisted extractions on fiber characteristics and properties. *Food Hydrocolloids, 123*, Article 107201.
Peters, J. P. C. M., Vergeldt, F. J., Boom, R. M., & van der Goot, A. J. (2017). Water-binding capacity of protein-rich particles and their pellets. *Food Hydrocolloids, 65*, 144–156.
Pillai, P. K., Guldiken, B., & Nickerson, M. T. (2021). Complex coacervation of pea albumin-pectin and ovalbumin-pectin assessed by isothermal titration calorimeter and turbidimetry. *Journal of the Science of Food and Agriculture, 101*(3), 1209–1217.
Pycarelle, S. C., Bosmans, G. M., Nys, H., Brijs, K., & Delcour, J. A. (2020). Stabilization of the air-liquid interface in sponge cake batter by surface-active proteins and lipids: A foaming protocol based approach. *Food Hydrocolloids, 101*, Article 105548.
Ran, X., & Yang, H. (2022). Promoted strain-hardening and crystallinity of a soy protein-konjac glucomannan complex gel by konjac glucomannan. *Food Hydrocolloids, 133*, Article 107959.
Renard, C. M. G. C., & Thibault, J.-F. (1993). Structure and properties of apple and sugar-beet pectins extracted by chelating agents. *Carbohydrate Research, 244*(1), 99–114.
Roque, A. M., Montinola, D., Geonzon, L., Matsukawa, S., Lobarbio, C. F. Y., Taboada, E. B., et al. (2022). Rheological elucidation of the viscoelastic properties and network interaction of mixed high-methoxyl pectin and kappa-carrageenan gels. *Food Hydrocolloids, 129*, Article 107647.
Sharma, M., Pondicherry, K. S., & Duizer, L. (2022). Understanding relations between rheology, tribology, and sensory perception of modified texture foods. *Journal of Texture Studies, 53*(3), 327–344.
Souza, C. J. F., & Garcia-Rojas, E. E. (2015). Effects of salt and protein concentrations on the association and dissociation of ovalbumin-pectin complexes. *Food Hydrocolloids, 47*, 124–129.
Sow, L. C., Nicole Chong, J. M., Liao, Q. X., & Yang, H. (2018). Effects of κ-carrageenan on the structure and rheological properties of fish gelatin. *Journal of Food Engineering, 239*, 92–103.
Sun, J., Li, X., Xu, X., & Zhou, G. (2011). Influence of various levels of flaxseed gum addition on the water-holding capacities of heat-induced porcine myofibrillar protein. *Journal of Food Science, 76*(3), C472–C478.
Synytsya, A. (2003). Fourier transform Raman and infrared spectroscopy of pectins. *Carbohydrate Polymers, 54*(1), 97–106.
van de Velde, F., de Hoog, E. H., Oosterveld, A., & Tromp, R. H. (2015). Protein-polysaccharide interactions to alter texture. *Annual Review of Food Science and Technology, 6*, 371–388.
Wang, J., Jiang, Q., Huang, Z., Muhammad, A. H., Gharsallaoui, A., Cai, M., et al. (2024). Rheological and mechanical behavior of soy protein-polysaccharide composite paste for extrusion-based 3D food printing: Effects of type and concentration of polysaccharides. *Food Hydrocolloids, 153*, Article 109942.
Wang, F., Lyu, J., Xie, J., & Bi, J. (2023). Texture formation of dehydrated yellow peach slices pretreated by osmotic dehydration with different sugars via cell wall pectin polymers modification. *Food Hydrocolloids, 134*, Article 108080.
Wang, J., Munk, M. B., Skibsted, L. H., & Ahrné, L. M. (2022). Impact of pectin and whey minerals solubilized by lime juice on calcium bioaccessibility in yogurt based snacks. *Food Hydrocolloids, 131*, Article 107817.
Wang, W., Shen, M., Jiang, L., Song, Q., Liu, S., & Xie, J. (2020). Influence of Mesona blumes polysaccharide on the gel properties and microstructure of acid-induced soy protein isolate gels. *Food Chemistry, 313*, Article 126125.
Wang, K., Sun, H., Cui, Z., Wang, J., Hou, J., Lu, F., et al. (2024). Synergistic effects of microbial transglutaminase and apple pectin on the gelation properties of pea protein isolate and its application to probiotic encapsulation. *Food Chemistry, 439*, Article 138232.
Wang, X., Zeng, M., Qin, F., Adhikari, B., He, Z., & Chen, J. (2018). Enhanced $CaSO_4$-induced gelation properties of soy protein isolate emulsion by pre-aggregation. *Food Chemistry, 242*, 459–465.
Wang, L., Zhang, M., Bhandari, B., & Gao, Z. (2016). Effects of malondialdehyde-induced protein modification on water functionality and physicochemical state of fish myofibrillar protein gel. *Food Research International, 86*, 131–139.
Warnakulasuriya, S., Pillai, P. K. S., Stone, A. K., & Nickerson, M. T. (2018). Effect of the degree of esterification and blockiness on the complex coacervation of pea protein isolate and commercial pectic polysaccharides. *Food Chemistry, 264*, 180–188.
Xie, J., Lyu, J., Wang, F., Bai, L., & Bi, J. (2024). Characterization of fruit pulp-soy protein isolate (SPI) complexes: Effect of superfine grinding. *Journal of Food Science, 89*(2), 1127–1142.
Xing, X., Chitrakar, B., Hati, S., Xie, S., Li, H., Li, C., et al. (2022). Development of black fungus-based 3D printed foods as dysphagia diet: Effect of gums incorporation. *Food Hydrocolloids, 123*, Article 107173.
Xue, H., Han, T., Zhang, G., Hu, X., Li, R., Liu, H., et al. (2023). Combined effects of NaOH, NaCl, and heat on the characteristics of ovalbumin gel and the exploration of the mechanism of transparent gel formation. *Food Hydrocolloids, 140*, Article 108589.
Yan, J., Li, S., Chen, G., Ma, C., McClements, D. J., Liu, X., et al. (2023). Formation, physicochemical properties, and comparison of heat- and enzyme-induced whey protein-gelatin composite hydrogels. *Food Hydrocolloids, 137*, Article 108384.
Yi, J., Gan, C., Wen, Z., Fan, Y., & Wu, X. (2021). Development of pea protein and high methoxyl pectin colloidal particles stabilized high internal phase pickering emulsions for β-carotene protection and delivery. *Food Hydrocolloids, 113*, Article 106497.
Yu, Q., Li, X., Hu, J., Wang, W., & Bi, J. (2023). The effect of three pectin fractions variation on the browning of different dried apple products. *Food Hydrocolloids, 134*, Article 108052.
Zhang, D., Chen, D., & Campanella, O. H. (2024). Effect of pH on the gelling properties of pea protein-pectin dispersions. *Food Hydrocolloids, 151*, Article 109731.
Zhang, H.-H., Huang, G.-Q., Geng, X., Teng, J., & Xiao, J.-X. (2021). Interaction between ovalbumin and pectin and coacervate characterization. *Colloid and Polymer Science, 299*(6), 943–953.
Zhang, X., Wang, Y., Li, Z., Li, Y., & Qi, B. (2024). Effects of polysaccharide type on the structure, interface behavior, and foam properties of soybean protein isolate hydrolysate-polysaccharide Maillard conjugates. *Food Hydrocolloids, 151*, Article 109801.
Zhou, M., Bi, J., Chen, J., Wang, R., & Richel, A. (2021). Impact of pectin characteristics on lipid digestion under simulated gastrointestinal conditions: Comparison of water-soluble pectins extracted from different sources. *Food Hydrocolloids, 112*, Article 106350.
Ekonomou, S.I., Hadnađev, M., Gioxari, A., Abosede, O. R., Soe, S., & Stratakos, A. C. (2024). Advancing dysphagia-oriented multi-ingredient meal development: Optimising hydrocolloid incorporation in 3D printed nutritious meals. *Food Hydrocolloids, 147*, Article 109300.